

Band alignment engineering of bilayer WS_2/Ga_2O_3 heterostructures with interface-dependent photoluminescence

YANG Wan-Li^{1,4}, HUANG Tian-Tian¹, ZHANG Le-Peng³, XU Pei-Ran¹, JIANG Cong¹, LI Tian-Xin¹,
CHEN Zhi-Min³, CHEN Xin^{1,2,4*}, DAI Ning^{1,2,4*}

1. State Key Laboratory of Infrared Physics, Shanghai Institute of Technical Physics, Chinese Academy of Sciences, Shanghai 200083, China;
2. Hangzhou Institute for Advanced Study, University of Chinese Academy of Sciences, Hangzhou 310024, China;
3. College of Materials Science and Engineering, Zhengzhou University, Zhengzhou 450052, China;
4. University of Chinese Academy of Sciences, Beijing 100049, China)

Abstract: The hetero-interface induced anomalous photoluminescence (PL) emissions in the vertical WS_2/Ga_2O_3 heterostructures was demonstrated. The WS_2/Ga_2O_3 hetero-interface varies type-II band structure and brings subsequent PL decline in the bottom WS_2 monolayer contacted with Ga_2O_3 layer. Such hetero-interlayer coupling interaction between oxides and 2D layered transition metal dichalcogenides (TMDs) in the stacked heterostructures impacts interlayer interaction between the bottom WS_2 monolayer and the upper WS_2 monolayer in a WS_2 bilayer, which leads to an anomalous PL enhancement in the bilayer WS_2 . Stacked hetero-interface will benefit for controlling the optical or electronic behavior and modulating energy band structures by customizing transformative 2D heterostructures used in next-generation nanoscale optoelectronic detectors and photodetectors.

Key words: WS_2 , Ga_2O_3 , heterostructure, interface, photoluminescence

具有界面依赖光致发光的双层 WS_2/Ga_2O_3 异质结的能带工程

杨万丽^{1,4}, 黄田田¹, 张乐鹏³, 徐沛然¹, 姜聪¹, 李天信¹, 陈志民³,
陈鑫^{1,2,4*}, 戴宁^{1,2,4*}

1. 中国科学院上海技术物理研究所 红外物理国家重点实验室, 上海 200083;
2. 国科大杭州高等研究院, 浙江 杭州 310024;
3. 郑州大学 材料科学与工程学院, 河南 郑州 450052;
4. 中国科学院大学, 北京 100049)

摘要: 利用垂直 WS_2/Ga_2O_3 异质结构中异质界面诱导了反常的光致发光(PL)发射。垂直堆栈的 WS_2/Ga_2O_3 异质界面使其形成了 II 型能带结构, 导致与 Ga_2O_3 层接触的底层 WS_2 的 PL 强度下降。而异质界面的强耦合作用也影响了双层 WS_2 中的同质层间相互作用, 使得上层 WS_2 出现反常的 PL 增强。这种堆栈新型二维异质结构为定制目标能带结构并控制其光子和电子行为提供一种新的手段。

关键词: 二硫化钨; 氧化镓; 异质结; 界面; 光致发光

中图分类号: O472+.3 文献标识码: A

Received date: 2022-09-14, revised date: 2022-12-22

收稿日期: 2022-09-14, 修回日期: 2022-12-22

Foundation items: Supported by National Natural Science Foundation of China (92064014, 11933006), Science and Technology Commission of Shanghai Municipality (18J1414900) and Youth Innovation Promotion Association CAS

Biography: YANG Wan-Li (1995-), female, Henan China, Ph. D. Research area involves semiconductor materials and devices. E-mail: yangwanli@mail.sitp.ac.cn

*Corresponding authors: E-mail: xinchen@mail.sitp.ac.cn, ndai@mail.sitp.ac.cn

Introduction

Stacked van der Waals heterostructures have extended versatile electrical, optical and chemical properties of individual 2D materials, and recently drawn broad attentions in optoelectronic detection and photodetection fields^[1-9]. The interfaces and interlayer interactions have shown significant impact on the energy band structure, charge transfer and density distribution, and defect formation in 2D heterostructures^[3-4, 10-14]. While the underlying physical mechanism still needs be further explored, 2D vertical heterostructures and interfacial engineering have become a promising platform to artificially design and manipulate desired atomic layered heterostructures and photodetectors. Notably, 2D TMDs (*e. g.*, MoS₂, WS₂) can emit pronounced photoluminescence (PL) by exciton recombination and release photons at room temperature^[11, 15]. Monolayer WS₂ possesses a direct band gap and abundant exciton behaviors for high PL quantum yield owing to strong light-matter coupling and thin dielectric screening in an atomic monolayer. However, the non-conservation of electron momentum will lead to a poor PL in a bilayer WS₂^[16-17]. The PL behaviors in 2D TMDs are determined by the energy band structure and exciton energy related to interlayer interaction, defects or doping. For a 2D interlayer stacking, the defect energy levels and bound excitons will also change energy band structure, transition behaviors of electrons and photons, and the proportion of excitons in TMDs^[18-20].

In van der Waals heterostructure, the interfacial interaction is ubiquitous and vital to significantly modulate and alter the optical and optoelectronic properties of 2D materials^[6, 21]. Hetero-interface strategies have provided a great opportunity to design and construct 2D stacked heterojunctions by band alignment engineering for the advanced microelectronic and optoelectronic detection devices^[9, 22]. It still remains challenging great to control complex and versatile interfaces in 2D homostructures and heterostructures. Various interface-engineering methods have been exploited to manipulate 2D heterostructures and their functions. Both CVD (*i. e.*, chemical vapor deposition) growth and mechanical transferring/stacking have been exploited to design and realize 2D van der Waals heterostructures on the desired substrates. Especially, during a CVD process, clean surface and original interface coupling can be feasibly obtained in 2D heterostructures^[10, 23-24]. Emerging 2D hetero-interfaces between TMDs and traditional semiconductors have sparked intensive interest in 2D heterostructures. Various Ga₂O₃ materials have been exploited to fabricate deep-ultraviolet photodetectors, functional FETs and high-power devices^[25-27]. Excellent electronic-photonic properties and high temperature-stability of Ga₂O₃ makes it possible to design and directly fabricate TMDs/oxide heterostructures.

In this work, we demonstrate an anomalous PL in the bilayer WS₂ induced by a hetero-interface between WS₂ layers and Ga₂O₃ thin films. In virtue of CVD-grown WS₂/Ga₂O₃ heterostructures on SiO₂/Si substrates, we analyzed surface-dependent PL and the role of interfaces.

Converse PL was found and anomalous in the region of bilayer-WS₂ on the Ga₂O₃ thin films. The PL intensity in the bilayer WS₂ (*i. e.*, 2L-WS₂) region is approximately 10 times stronger than that in the monolayer WS₂ (*i. e.*, 1L-WS₂) region. Such anomalous PL behaviors in bilayer WS₂ depend on hetero-interface and modified energy band structures in the WS₂/Ga₂O₃ heterostructure. WS₂/oxide hetero-interfaces provide an alternative route to understand and manipulate the optical and electronic behaviors of 2D vertical heterostructures and functional detection devices.

1 Materials and methods

The 2D WS₂/Ga₂O₃ vertical heterostructures are directly fabricated by a CVD method. In brief, the Ga₂O₃ thin films were atomic-layer-deposited on the SiO₂/Si substrates as we reported elsewhere^[26-27]. The layered WS₂ was subsequently CVD-grown on the as-prepared Ga₂O₃ thin film, which may help for a clean hetero-interface in WS₂/Ga₂O₃ vertical heterostructure. Thus, WO₃ and S powders were used as precursors during the CVD-growth of 2D WS₂ and WS₂/Ga₂O₃ heterostructures grown at ~ 850 °C. High-resolution Raman/PL maps were obtained with 100 × objective, 1 800/300 G/mm grating, and a scanning step of 300 nm while the intensity of 532 nm laser is less than 1 mW. Raman/PL spectroscopy was performed at room temperature. To fabricate transferred-WS₂/Ga₂O₃ heterostructure, the target WS₂ flakes on the SiO₂/Si substrate were pasted on a cut polyvinyl alcohol hydrogel sheet, and then transferred onto the Ga₂O₃ thin film on SiO₂/Si substrate according to the processes reported elsewhere. Briefly, KPFM image was obtained on Veeco/DI multimode SPM while optical microscopy was performed on Leica DM4000M^[28-29].

2 Results and discussions

Figure 1 (a) displays a schematic illustration of the 2D WS₂/Ga₂O₃ vertical heterostructure on SiO₂/Si substrates. Here, the bottom monolayer in bilayer-WS₂ contacted Ga₂O₃ thin film was referred as first layer WS₂ (*i. e.*, 1stL-WS₂) while the upper layer as second layer WS₂ (*i. e.*, 2ndL-WS₂). Generally, the PL intensity of the 1stL-WS₂ is much stronger than that of the 2ndL-WS₂ in the bilayer-WS₂ obtained on SiO₂/Si substrates^[16]. Nonetheless, an entire converse PL phenomenon was found from PL intensity map (at 640 nm) of the bilayer-WS₂/Ga₂O₃ heterostructure, as shown in Fig. 1 (b). The PL intensity in the 2L-WS₂ domain surrounded by the white dashed triangle is evidently much stronger than that in the 1L-WS₂ domain. Figure 1 (c) shows obvious contrast PL spectra in the 1L-WS₂ and 2L-WS₂ domains. The inset reveals that the PL intensity in the 2L-WS₂ domain is approximately 10 times stronger than the intensity in the 1L-WS₂ domain. Notably, the anomalous PL emissions were observed in at least six cases of CVD-grown WS₂/Ga₂O₃ heterostructures, where the stronger PL intensity of 2L-WS₂ is than that of 1L-WS₂. Subsequently, we further focused on such anomalous PL enhancement and the roles of the hetero-interface between Ga₂O₃ and the 1stL-

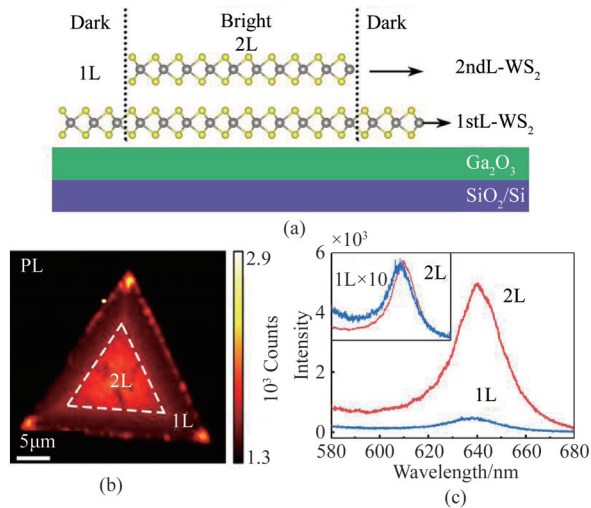


Fig. 1 (a) Structural model schematic illustration of bilayer- $\text{WS}_2/\text{Ga}_2\text{O}_3$ heterostructure, (b) PL intensity map (at a wavelength of 640 nm) of layered WS_2 on Ga_2O_3 thin film, (c) PL spectra of the 1 L- WS_2 and 2 L- WS_2 domains in the heterostructure shown in (b)

图1 (a) 双层 $\text{WS}_2/\text{Ga}_2\text{O}_3$ 异质结的结构示意图, (b) Ga_2O_3 薄膜上层状 WS_2 的 PL 强度图 (在 640 nm), (c) 图(b) 异质结中 1 L- WS_2 和 2 L- WS_2 的 PL 光谱

WS_2 , and the homo-interface between the 1stL- WS_2 and the 2ndL- WS_2 in the bilayer- $\text{WS}_2/\text{Ga}_2\text{O}_3$ heterostructure.

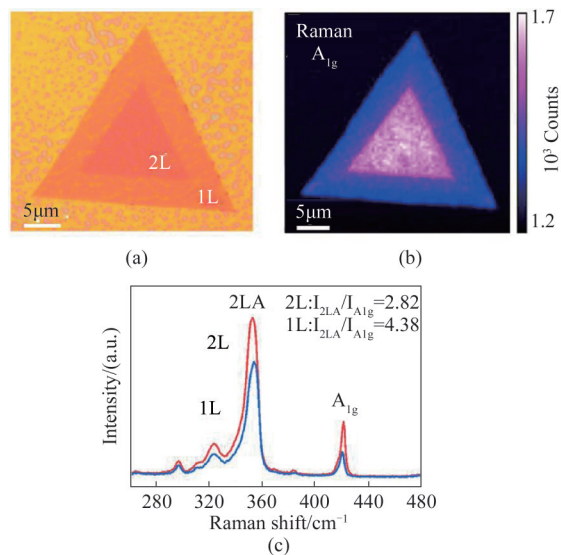


Fig. 2 (a) Optical microscopy image of bilayer $\text{WS}_2/\text{Ga}_2\text{O}_3$ heterostructure, (b) corresponding Raman A_{1g} mode intensity map of bilayer- WS_2 on Ga_2O_3 thin film in (a), the blue region is the 1 L region marked in (a) while the 2 L region is shown as the red, (c) Raman spectra of 1L- WS_2 and 2L- WS_2 in the heterostructure

图2 (a) 双层 $\text{WS}_2/\text{Ga}_2\text{O}_3$ 异质结的光学显微镜照片, (b) 对应图(a) Ga_2O_3 薄膜上双层 WS_2 的 Raman A_{1g} 强度图, 蓝色区域为 1 L 而红色区域为 2 L, (c) 异质结中 1L- WS_2 和 2L- WS_2 的 Raman 光谱

Interlayer interactions and interfaces affect and even determine PL emission of 2D materials^[17, 30]. Therefore, we thought that the hetero-interlayer coupling between

the bottom Ga_2O_3 -layer and the 1stL- WS_2 layer might play an important role in the anomalous PL. The PL emission intensity of 1L- WS_2 decreases as displayed in Fig. 1(c), which might relate with the energy band structure and changed crystal lattice of the 1stL- WS_2 ^[31]. The $\text{WS}_2/\text{Ga}_2\text{O}_3$ hetero-interface should be different from those in the WS_2/SiO_2 and 1stL/2ndL WS_2 cases due to some possible changes in dielectric interfaces and interlayer spacing^[32]. Such $\text{WS}_2/\text{Ga}_2\text{O}_3$ hetero-interface might change the homo-interlayer coupling between the 1stL- WS_2 and the 2ndL- WS_2 , which leads to a special 1L- WS_2 and 2L- WS_2 different from that in the cases of monolayer WS_2 and bilayer- WS_2 on the SiO_2/Si substrates. As a consequence, all of these may lead to a stronger PL emission in the 2L- WS_2 region while a weaker one in the 1L- WS_2 .

Figure 2 further shows optical image and Raman measurements of the 1st-layer and the 2nd-layer WS_2 region in the bilayer $\text{WS}_2/\text{Ga}_2\text{O}_3$ heterostructure. As represented in Fig. 2(a), 1L- WS_2 and 2L- WS_2 domains are easily distinguished from the optical contrast. In Raman spectra, the in-plane shear vibration ($2LA$ and E_{2g}^1) and the out-plane layer breathing vibration (A_{1g}) locate at $\sim 350 \text{ cm}^{-1}$ and $\sim 420 \text{ cm}^{-1}$, respectively^[33]. In addition, for the vibration peak at $\sim 350 \text{ cm}^{-1}$, the second-order $2LA$ mode is dominant due to the double-resonance process^[34]. Moreover, varying with layer number, the intensity of A_{1g} mode (Fig. 2(b)) is effectively discriminated in the Raman map in Fig. 2(b). The A_{1g} peak intensity of 2L- WS_2 (pink region) is stronger than that of 1L- WS_2 (blue region). The ratio of the intensities of two characteristic peaks (*i. e.*, $I_{2LA}/I_{A_{1g}}$) is calculated and approximately 4.38 for the 1L- WS_2 while that is about 2.82 for the 2L- WS_2 (Fig. 2(c)). The value of $I_{2LA}/I_{A_{1g}}$ decreased as the layer number increased, and then was exploited to further check and distinguish 1L- WS_2 and 2L-layer WS_2 as reported elsewhere^[35].

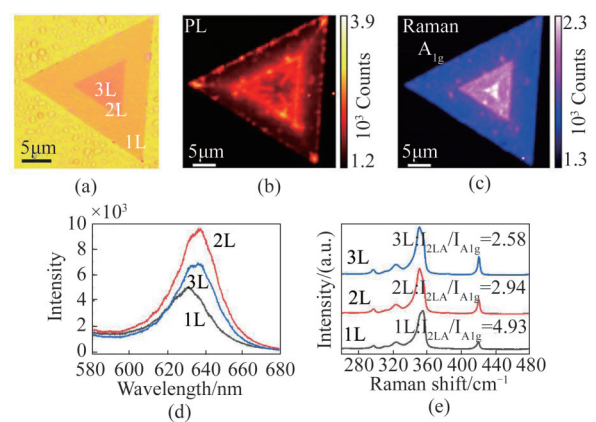


Fig. 3 (a) Optical image of trilayer- $\text{WS}_2/\text{Ga}_2\text{O}_3$ heterostructure, (b) PL intensity map of WS_2 on Ga_2O_3 thin film, (c) Raman A_{1g} mode intensity map of WS_2 on Ga_2O_3 thin film, (d) PL and (e) Raman spectra of 1 L- WS_2 , 2 L- WS_2 and 3 L- WS_2 in the heterostructure shown in (a)

图3 (a) 三层 $\text{WS}_2/\text{Ga}_2\text{O}_3$ 异质结的光学显微镜照片, (b) Ga_2O_3 薄膜上 WS_2 的 PL 强度图, (c) Ga_2O_3 薄膜上 WS_2 的 Raman A_{1g} 强度图, 图(a) 异质结中 1 L- WS_2 , 2 L- WS_2 和 3 L- WS_2 的 (d) PL 光谱和 (e) Raman 光谱

For further comparison, a trilayer-WS₂/Ga₂O₃ heterostructure were checked and investigated as suggested in Fig. 3. Optical contrast in Fig. 3(a) changes and is different in the 1L, 2L, and 3L-WS₂ domains. Raman intensity map in Fig. 3(c) also displays and manifests the corresponding 1L-WS₂ (blue region), 2L-WS₂ (pink region) and 3L-WS₂ (white region) domains. As mentioned above, the intensity of A_{1g} vibration increases with layer number. The value of $I_{2LA}/I_{A_{1g}}$ decreases with the increase of layer number, and is approximately 4.93, 2.94, and 2.58 for 1L-WS₂, 2L-WS₂ and 3L-WS₂, respectively. Typically, the value of $I_{2LA}/I_{A_{1g}}$ is more than 5 for a WS₂ monolayer on SiO₂/Si substrate, but it is less than 5 for that of 1L-WS₂ in WS₂/Ga₂O₃ heterostructure, which implies that the vibration mode of 1L-WS₂ may be changed by the hetero-interface between Ga₂O₃ and 1stL-WS₂^[35].

Furthermore, the PL intensity of trilayer-WS₂ on Ga₂O₃ reveals the dark-bright-dark alternating arrangement from accordant outer-1L to inner-3L as indicated in the PL intensity map in Fig. 3(b). The respective PL spectra are extracted from PL intensity map, as shown in Fig. 3(d). We noted that the PL intensity of 2L-WS₂ is higher than that of 3L-WS₂ while the one of 1L-WS₂ is the lowest. Moreover, a redshift of ~5 nm in the PL between 1L-WS₂ and 2L-WS₂ is shown in Fig. 3(d), and but such shifts do not occur in the case of trilayer-WS₂ on the SiO₂/Si substrate. All these convincingly suggest that the hetero-interface between 1stL-WS₂ and underlying Ga₂O₃ thin film plays a critical role in changing and weakening PL of 1L-WS₂. The hetero-interface between the bottom 1stL-WS₂ and the underlying Ga₂O₃ thin film might reduce the homo-interlayer coupling between 1stL-WS₂ and 2ndL-WS₂.

Monolayer-WS₂/Ga₂O₃ heterostructure in Fig. 4 is used to further check and certify the role of hetero-inter-

face. The optical contrast of OM image (Fig. 4(a)) and intensity consistency of PL/Raman maps (Fig. 4(b) and 4(c)) display and confirm the monolayer-WS₂/Ga₂O₃ heterostructure. Figure 4(e) implies that the $I_{2LA}/I_{A_{1g}}$ value of the WS₂ monolayer in monolayer-WS₂/Ga₂O₃ heterostructure is approximately 4.00 from Raman spectra, which also results from the WS₂/Ga₂O₃ interface interaction as mentioned above. In addition, the PL intensity of monolayer-WS₂ in the heterostructure in Fig. 4(d) is less than that of monolayer-WS₂ on the SiO₂/Si substrate. Notably, the PL intensity of 1L-WS₂ in bilayer-WS₂/Ga₂O₃ heterostructure (Fig. 1c) is less than that of the WS₂ monolayer (Fig. 4(d)). In addition, the PL intensity of 2L-WS₂ is stronger than both the one of 1L-WS₂ in bilayer-WS₂/Ga₂O₃ heterostructure (Fig. 1c) and that of the WS₂ monolayer (Fig. 4(d)). All these results reveal that the presence of 2L-WS₂ in bilayer-WS₂/Ga₂O₃ heterostructure may further weaken the PL intensity of the 1L-WS₂ in bilayer-WS₂/Ga₂O₃ heterostructure. The varied energy band structure and possible interlayer charge transfer in both 1L-WS₂ and 2L-WS₂ may play an important role in an increasing PL intensity of 2L-WS₂ and a weaken PL intensity in the bilayer-WS₂/Ga₂O₃ heterostructure.

It has been documented that different contacted materials means different interfaces and dielectric environments^[13, 36-38]. Figure 5 shows the PL variation in the trilayer-WS₂ on SiO₂/Si substrate, and further verifies the roles of different interfaces on the PL intensity distribution of layered WS₂. Figure 5(a) displays the different layer-domains distribution and the optical contrast in the trilayer-WS₂ on SiO₂/Si substrate. As illustrated in Fig. 5(b), the 1L-WS₂ on SiO₂/Si substrate displays the strongest PL emission, which is far outweighing that of 2L-WS₂ and 3L-WS₂. Thus, it is hard to distinguish the 2L and 3L-WS₂ domains in Fig. 5(b). Figure 5(c) shows the Raman map of trilayer-WS₂ on the SiO₂/Si substrate and the different layer-domains marked by dashed triangles.

PL spectra of each layer in the trilayer-WS₂ on SiO₂/Si substrate are taken from Fig. 5(b) and then represented in Fig. 5(d). The PL intensity in 1L region is much larger than that in 2L and 3L regions because the PL intensity of WS₂ decreases sharply with the increase of the layer number. Monolayer WS₂ possesses direct band gap while bilayer and few layers WS₂ are generally indirect band gap. Notably, the PL peak position of each layer in the trilayer-WS₂ on SiO₂/Si substrate is near 630 nm. Figure 5(e) shows the values of $I_{2LA}/I_{A_{1g}}$ for 1L-WS₂, 2L-WS₂ and 3L-WS₂ is approximately 6.59, 4.52, 1.74, respectively. Here, the $I_{2LA}/I_{A_{1g}}$ value of the 1L-WS₂ in the trilayer-WS₂ on SiO₂/Si substrate is larger than 5. All these are different from those in the case of the trilayer-WS₂/Ga₂O₃ heterostructure above, and further suggest that the hetero-interface between Ga₂O₃ thin film and WS₂ definitely affects the optical band gap of WS₂.

To further prove and understand the role of WS₂/Ga₂O₃ hetero-interfaces on PL emission of WS₂, we also constructed transferred-bilayer-WS₂/Ga₂O₃ heterostruc-

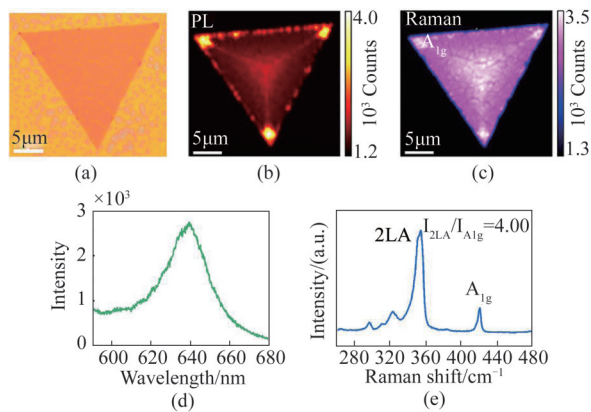


Fig. 4 (a) Optical image of monolayer-WS₂/Ga₂O₃ heterostructure, (b) PL intensity map of WS₂ on Ga₂O₃ thin film, (c) Raman A_{1g} mode intensity map of WS₂ on Ga₂O₃ thin film, (d) PL spectrum and (e) Raman spectrum of WS₂ in monolayer WS₂/Ga₂O₃ heterostructure

图4 (a) 单层 WS₂/Ga₂O₃ 异质结的光学显微镜照片, (b) Ga₂O₃ 薄膜上 WS₂ 的 PL 强度图, (c) Ga₂O₃ 薄膜上 WS₂ 的 Raman A_{1g} 强度图; 单层 WS₂/Ga₂O₃ 异质结中 WS₂ 的 (d) PL 光谱和 (e) Raman 光谱

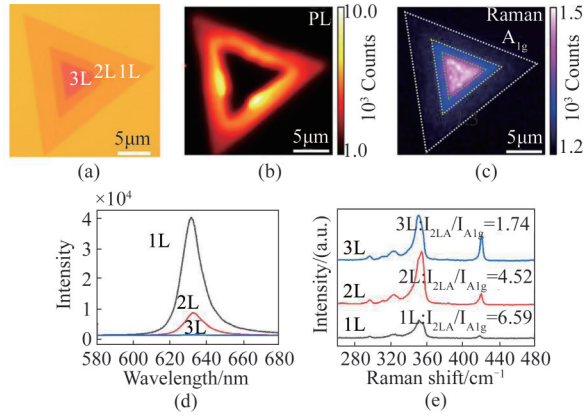


Fig. 5 (a) Optical image of trilayer-WS₂ on the SiO₂/Si substrate, (b) PL intensity map of WS₂ on the SiO₂/Si substrate, (c) Raman A_{1g} mode intensity map of WS₂ on the SiO₂/Si substrate, (d) PL and (e) Raman spectra of 1L-WS₂, 2L-WS₂ and 3L-WS₂ shown in (a)

图5 (a) SiO₂/Si衬底上三层WS₂的光学显微镜照片, (b) SiO₂/Si衬底上WS₂的PL强度图, (c) SiO₂/Si衬底上WS₂的Raman A_{1g}强度图, 图(a)中1L-WS₂、2L-WS₂和3L-WS₂的(d) PL光谱和(e) Raman光谱

ture (Fig. 6) similar with Fig. 1(a) by transferring a 2L-WS₂ from SiO₂/Si substrate to the annealed Ga₂O₃ thin film. Raman, PL and OM images were obtained on the transferred-bilayer-WS₂/Ga₂O₃ heterostructure, and further used to understand the hetero-interlayer coupling in WS₂/Ga₂O₃ heterostructures. The transferred-bilayer-WS₂/Ga₂O₃ heterostructure can be observed from the OM image and PL/Raman maps. We noted that the PL intensity map (Fig. 6(b)) is similar to that in the case of the layered WS₂ on SiO₂/Si substrates. The intensity of 1L-WS₂ domain is much stronger than that in 2L-WS₂ domain in the transferred-bilayer-WS₂/Ga₂O₃ heterostructure (Fig. 6(d)) while the PL behaviors of 1L-WS₂ and even 2L-WS₂ do not change. Notably, the anomalous PL emissions, that is the PL intensity of 2L-WS₂ is stronger than that of 1L-WS₂, were observed in at least 6 samples. All these confirm the critical effects of WS₂/Ga₂O₃ hetero-interfaces on the anomalous PL behaviors of WS₂ in the bilayer-WS₂/Ga₂O₃ heterostructure. In addition, the I_{2LA}/I_{A1g} value for 1L-WS₂ in the transferred-bilayer-WS₂/Ga₂O₃ heterostructure is approximately 7.98 while the one for 2L-WS₂ is about 4.69 (Fig. 6(e)). The unavoidable interface contaminations during transferring process affected the interfacial coupling^[20, 39].

Subsequently, two peaks can be fitted by Lorentz model and assigned to neutral excitons and negative trions, which help study the distinctive PL emission behaviors in bilayer WS₂/Ga₂O₃ heterostructure. The PL spectra of 1L and 2L-WS₂ on different substrates are displayed in Fig. 1(c) and Fig. 5(e). The intensity ratio of trions and excitons ($I_{trion}/I_{exciton}$) of the WS₂ on Ga₂O₃ is greater than that on SiO₂/Si. It means that trions dominate the PL emission of WS₂ layer contacted with Ga₂O₃ thin film, which reveals that the charge density of WS₂ in WS₂/Ga₂O₃ heterostructure is higher. It is well-known that more electrons can be bonding with neutral excitons

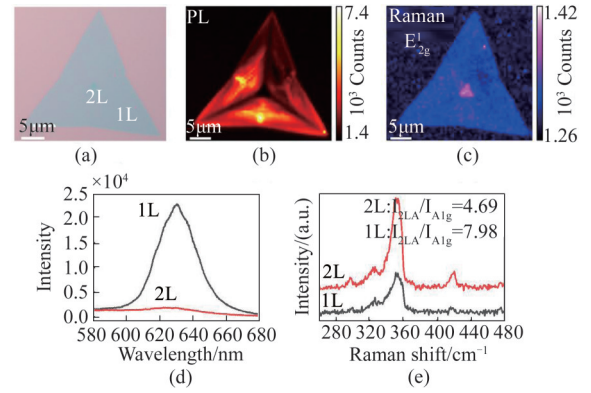


Fig. 6 (a) Optical image of transferred bilayer-WS₂/Ga₂O₃ heterostructure, (b) PL intensity map of WS₂ transferred on Ga₂O₃ thin film, (c) Raman A_{1g} mode intensity map of WS₂ transferred on Ga₂O₃ thin film, (d) PL and (e) Raman spectra of 1L-WS₂ and 2L-WS₂ in the heterostructure shown in (a)

图6 (a) 转移的双层WS₂/Ga₂O₃异质结的光学显微镜照片, (b) 转移到Ga₂O₃薄膜上的WS₂的PL强度图, (c) 转移到Ga₂O₃薄膜上的WS₂的Raman A_{1g}强度图, 图(a)异质结中1L-WS₂和2L-WS₂的(d) PL光谱和(e) Raman光谱

to form more trions, which may reduce PL emission. Then, the I_{2LA}/I_{A1g} value is weak in the case of WS₂ grown on Ga₂O₃ because of the enhancement of A_{1g} mode, and relates to the n-type doping and interfacial distance, where produce more trions. The interfacial distance affects charges doping and transferring between WS₂ and Ga₂O₃ in WS₂/Ga₂O₃ heterostructures^[40-41], which reveals a stronger interfacial interaction in grown-WS₂/Ga₂O₃ heterostructures.

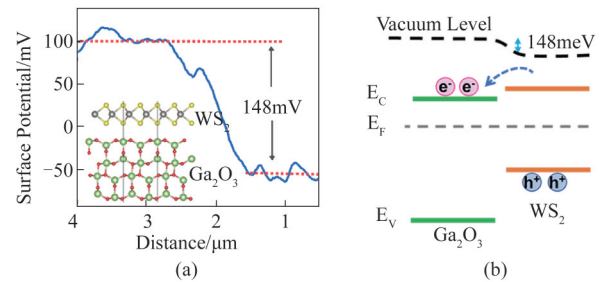


Fig. 7 (a) Surface potential (KPFM) profile of WS₂/Ga₂O₃ heterostructure, inset image is schematic diagram of WS₂/Ga₂O₃ heterostructure, (b) schematic of the energy band structure of WS₂/Ga₂O₃ heterostructure

图7 (a) WS₂/Ga₂O₃异质结的表面电势分布, 插图为WS₂/Ga₂O₃异质结的原子结构示意图, (b) WS₂/Ga₂O₃异质结的能带结构示意图

We further exploited Kelvin probe force microscopy (KPFM) to check and identify varied surface potential in WS₂/Ga₂O₃ heterostructures for understanding their optical behaviors (Fig. 7). The theoretical energy bands calculated by density function theory suggested the formation of type-II heterojunctions between layered WS₂ and Ga₂O₃ thin film, which may result in an indirect-band WS₂ monolayer in WS₂/Ga₂O₃ heterostructures. Furthermore, the presence of type-II band alignments in heterojunctions leads to layer-separated electrons and hole car-

riers in two different materials, and then to a sudden fall of PL emission. We noted that the surface potential difference was approximately 148 mV between WS₂ and Ga₂O₃, which helped electron-transferring from the WS₂ layer to the Ga₂O₃ layer in the WS₂/Ga₂O₃ heterostructure. All these processes depend on the interlayer charge transfer and intralayer recombination competition^[42-43], and then cause consequent variations of Raman and PL spectra. In fact, the interfacial interaction affects and even dominates the optical and electrical behaviors (*e. g.*, enhanced or reduced PL emission) in van der Waals heterostructures^[24]. The strong PL suppression in Fig. 4 compared with that of Fig. 5 indicated the strong coupling in the WS₂/Ga₂O₃ heterostructure.

There are several synergistic determinants for the interlayer coupling, including interface composition, defects, the twist angle, the charge transfer, the interfacial charge traps, original internal stress and other possible factors^[31-32, 36, 44-48]. For the WS₂/Ga₂O₃ heterostructures, the anomalous PL behaviors in the WS₂ bilayer depended on the hetero-interfaces between bilayer-WS₂ and Ga₂O₃. The decreased interlayer spacing and the strong hetero-interfacial interaction between 1stL-WS₂ and Ga₂O₃ were possibly caused by the interfacial defects and doping, the covalent bonding or enhanced van der Waals force^[23-24]. Moreover, the WS₂/Ga₂O₃ hetero-interfaces may change interlayer spacing and then effect the homo-interlayer coupling between two near monolayers in bilayer or trilayer WS₂. All these may alter the energy band structure and PL behaviors of 2L-WS₂^[18-20, 34]. Although the dynamics mechanism of the PL in WS₂ hetero-interface needs further exploration, these investigations will extend an alternative prospect of understanding the function of the interfacial interaction and constructing vertical TMDs/oxide stacking with excellent optical and electronic performances.

3 Conclusions

In summary, we demonstrated the anomalous PL behaviors in CVD-grown bilayer WS₂ in a 2D stacking WS₂/Ga₂O₃ heterostructure. Various hetero-interfaces and interfacial interactions were explored and uncovered to determine unconditional PL emissions in WS₂/Ga₂O₃ heterostructures. Strong WS₂/Ga₂O₃ hetero-interfacial coupling affects 1stL-WS₂/2ndL-WS₂ interlayer interactions and weakens PL emissions of 1L-WS₂ for a PL enhancement in bilayer WS₂. Ongoing investigations focus on the interface-dependent PL dynamics in WS₂/Ga₂O₃ heterostructures. Such heterointerface-dependent anomalous PL behaviors will provide more opportunities for modulating energy band structures and the optical or electronic properties of 2D stacked heterostructures, and may benefit for next-generation nanoscale TMDs/oxide-based optoelectronic detectors and photodetection.

Acknowledgment

The authors thank X. H. Zhou and X. Ge for their

help with DFT calculations and discussions.

References

- [1] Jariwala D, Marks T J, Hersam M C. Mixed-dimensional van der Waals heterostructures [J]. *Nature Materials*, 2017, **16** (2) : 170-181.
- [2] Li D, Li Z, Chen P, *et al.* Two-dimensional metal chalcogenide heterostructures: Designed growth and emerging novel applications [J]. *Advanced Materials Interfaces*, 2021, **8**(15):2100515.
- [3] Duong D L, Yun S J, Lee Y H. Van der Waals layered materials: Opportunities and challenges [J]. *ACS Nano*, 2017, **11** (12) : 11803-11830.
- [4] Lu Z, Neupane G P, Jia G, *et al.* 2D materials based on main group element compounds: Phases, synthesis, characterization, and applications [J]. *Advanced Functional Materials*, 2020, **30** (40) : 2001127.
- [5] Mueller T, Malic E. Exciton physics and device application of two-dimensional transition metal dichalcogenide semiconductors [J]. *npj 2D Materials and Applications*, 2018, **2**(1):29.
- [6] Zhou X, Hu X, Yu J, *et al.* 2D layered material-based van der Waals heterostructures for optoelectronics [J]. *Advanced Functional Materials*, 2018, **28**(14):1706587.
- [7] Liu R, Wang F, Liu L, *et al.* Band alignment engineering in two-dimensional transition metal dichalcogenide-based heterostructures for photodetectors [J]. *Small Structures*, 2020, **2**(3) :2000136.
- [8] Yang X, Qin T, Zhang X, *et al.* Self-crystallized interlayer integrating polysulfide-adsorbed TiO₂/TiO and highly-electron-conductive TiO for high-stability lithium-sulfur batteries [J]. *Chemical Research in Chinese Universities*, 2020, **37**(2) :259-264.
- [9] Jiang J, Wen Y, Wang H, *et al.* Recent advances in 2D materials for photodetectors [J]. *Advanced Electronic Materials*, 2021, **7** (7) : 2001125.
- [10] Hong H, Liu C, Cao T, *et al.* Interfacial engineering of van der Waals coupled 2D layered materials [J]. *Advanced Materials Interfaces*, 2017, **4**(9):1601054.
- [11] Lee J Y, Shin J H, Lee G H, *et al.* Two-dimensional semiconductor optoelectronics based on van der Waals heterostructures [J]. *Nanomaterials*, 2016, **6**(11):193.
- [12] Zavabeti A, Jannat A, Zhong L, *et al.* Two-dimensional materials in large-areas: Synthesis, properties and applications [J]. *Nano-Micro Letters*, 2020, **12**(1):66.
- [13] Raja A, Chaves A, Yu J, *et al.* Coulomb engineering of the bandgap and excitons in two-dimensional materials [J]. *Nature Communications*, 2017, **8**:15251.
- [14] Bae S H, Kum H, Kong W, *et al.* Integration of bulk materials with two-dimensional materials for physical coupling and applications [J]. *Nature Materials*, 2019, **18**(6):550-560.
- [15] Zhang X, Qiao X, Shi W, *et al.* Phonon and Raman scattering of two-dimensional transition metal dichalcogenides from monolayer, multilayer to bulk material [J]. *Chemical Society Reviews*, 2015, **44** (9):2757-2785.
- [16] Li Y, Li X, Yu T, *et al.* Accurate identification of layer number for few-layer WS₂ and WSe₂ via spectroscopic study [J]. *Nanotechnology*, 2018, **29**(12):124001.
- [17] Luong D H, Lee H S, Neupane G P, *et al.* Tunneling photocurrent assisted by interlayer excitons in staggered van der Waals hetero-bilayers [J]. *Advanced Materials*, 2017, **29**(33):1701512.
- [18] Kaul A B. Two-dimensional layered materials: Structure, properties, and prospects for device applications [J]. *Journal of Materials Research*, 2014, **29**(3):348-361.
- [19] Raja A, Selig M, Berghauer G, *et al.* Enhancement of exciton-phonon scattering from monolayer to bilayer WS₂ [J]. *Nano Letters*, 2018, **18**(10):6135-6143.
- [20] Zhou Y, Tan H, Sheng Y, *et al.* Utilizing interlayer excitons in bilayer WS₂ for increased photovoltaic response in ultrathin graphene vertical cross-bar photodetecting tunneling transistors [J]. *ACS Nano*, 2018, **12**(5):4669-4677.
- [21] Zhang H, Wu W, Zhou L, *et al.* Steering on degrees of freedom of 2D van der Waals heterostructures [J]. *Small Science*, 2021, **2**(1) : 2100033.
- [22] Ahmad W, Liu J, Jiang J, *et al.* Strong interlayer transition in few-layer InSe/PdSe₂ van der Waals heterostructure for near-infrared photodetection [J]. *Advanced Functional Materials*, 2021, **31** (43) : 2104143.

- [23] Liu X, Hersam M C. Interface characterization and control of 2D materials and heterostructures [J]. *Advanced Materials*, 2018, **30**(39): e1801586.
- [24] Shi Z, Wang X, Sun Y, *et al.* Interlayer coupling in two-dimensional semiconductor materials [J]. *Semiconductor Science and Technology*, 2018, **33**(9):093001.
- [25] Cui H, Sai Q, Qi H, *et al.* Analysis on the electronic trap of β -Ga₂O₃ single crystal [J]. *Journal of Materials Science*, 2019, **54**(19):12643–12649.
- [26] Liu W, Zhu X, He J, *et al.* Atomic-layer-Ti-doped Ga₂O₃ thin films with tunable optical properties and wide ultraviolet optoelectronic responses [J]. *Physica Status Solidi RRL: Rapid Research Letters*, 2021, **15**(11):2100411.
- [27] Yang Y, Liu W, Huang T, *et al.* Low deposition temperature amorphous ALD-Ga₂O₃ thin films and decoration with MoS₂ multilayers toward flexible solar-blind photodetectors [J]. *ACS Applied Materials & Interfaces*, 2021, **13**(35):41802–41809.
- [28] Zhang K, Zhang T, Cheng G, *et al.* Interlayer transition and infrared photodetection in atomically thin type-II MoTe₂/MoS₂ van der Waals heterostructures [J]. *ACS Nano*, 2016, **10**(3):3852–3858.
- [29] Yang W, Huang T, He J, *et al.* Monolayer WS₂ lateral homosuperlattices with two-dimensional periodic localized photoluminescence [J]. *ACS Nano*, 2022, **16**(1):597–603.
- [30] He Z, Sheng Y, Rong Y, *et al.* Layer-dependent modulation of tungsten disulfide photoluminescence by lateral electric fields [J]. *ACS Nano*, 2015, **9**(3):2740–2748.
- [31] Xiang Q, Yue X, Wang Y, *et al.* Unveiling the origin of anomalous low-frequency Raman mode in CVD-grown monolayer WS₂ [J]. *Nano Research*, 2021, **14**(11):4314–4320.
- [32] Zhang J, Wang J, Chen P, *et al.* Observation of strong interlayer coupling in MoS₂/WS₂ heterostructures [J]. *Advanced Materials*, 2016, **28**(10):1950–1956.
- [33] Liang L, Zhang J, Sumpter B G, *et al.* Low-frequency shear and layer-breathing modes in Raman scattering of two-dimensional materials [J]. *ACS Nano*, 2017, **11**(12):11777–11802.
- [34] Zeng H, Liu G B, Dai J, *et al.* Optical signature of symmetry variations and spin-valley coupling in atomically thin tungsten dichalcogenides [J]. *Scientific Reports*, 2013, **3**:1608.
- [35] Matthews S, Zhao C, Zeng H, *et al.* Effects of acetone vapor on the exciton band photoluminescence emission from single- and few-layer WS₂ on template-stripped gold [J]. *Sensors*, 2019, **19**(8):1913.
- [36] Hong X, Kim J, Shi S F, *et al.* Ultrafast charge transfer in atomically thin MoS₂/WS₂ heterostructures [J]. *Nature Nanotechnology*, 2014, **9**(9):682–686.
- [37] Khan Y, Obaidulla S M, Rezwan Habib M, *et al.* Anomalous photoluminescence quenching in DIP/MoS₂ van der Waals heterostructure: Strong charge transfer and a modified interface [J]. *Applied Surface Science*, 2020, **530**:147213.
- [38] Li K, Wang W. Effects of substrates on the optical properties of monolayer WS₂ [J]. *Journal of Crystal Growth*, 2020, **540**:125645.
- [39] Carey B J, Ou J Z, Clark R M, *et al.* Wafer-scale two-dimensional semiconductors from printed oxide skin of liquid metals [J]. *Nature Communications*, 2017, **8**:14482.
- [40] Choi S H, Choi J H, Oh C S, *et al.* Universal transfer of 2D materials grown on Au substrate using sulfur intercalation [J]. *Applied Science and Convergence Technology*, 2021, **30**(2):45–49.
- [41] Das S, Chowdhury R K, Karmakar D, *et al.* Substrate-dependent synergistic many-body effects in atomically thin two-dimensional WS₂ [J]. *Physical Review Materials*, 2021, **5**(12):124001.
- [42] Choi W, Ahn J, Kim K T, *et al.* Ambipolar channel p-TMD/n-Ga₂O₃ junction field effect transistors and high speed photo-sensing in TMD channel [J]. *Advanced Materials*, 2021, **33**(38):e2103079.
- [43] Zheng B, Ma C, Li D, *et al.* Band alignment engineering in two-dimensional lateral heterostructures [J]. *Journal of the American Chemical Society*, 2018, **140**(36):11193–11197.
- [44] Lau C S, Chee J Y, Cao L, *et al.* Gate-defined quantum confinement in CVD 2D WS₂ [J]. *Advanced Materials*, 2021, **34**(25):e2103907.
- [45] Yang S, Luo P, Wang F, *et al.* Van der Waals epitaxy of Bi₂Te₂Se/Bi₂O₂Se vertical heterojunction for high performance photodetector [J]. *Small*, 2021, **18**(6):e2105211.
- [46] Peng Q, Ge X, Wang R, *et al.* Investigation of carrier migration from WS₂ monolayer to substrate by photoluminescence [J]. *Journal of Luminescence*, 2022, **241**:118538.
- [47] Zhang K, Guo Y, Larson D T, *et al.* Spectroscopic signatures of interlayer coupling in janus MoSSe/MoS₂ heterostructures [J]. *ACS Nano*, 2021, **15**(9):14394–14403.
- [48] Tan Q, Rasmita A, Li S, *et al.* Layer-engineered interlayer excitons [J]. *Science of Advanced*, 2021, **7**(30):eabh0863.